THE ASTROPHYSICAL JOURNAL, 451:825–842, 1995 October 1

THE INFLUENCE OF A VERTICAL MAGNETIC FIELD ON OSCILLATIONS IN AN ISOTHERMAL STRATIFIED ATMOSPHERE. II.

DIPANKAR BANERJEE AND S. S. HASAN
Indian Institute of Astrophysics, Sarjapur Road, Bangalore 560034, India

AND

J. CHRISTENSEN-DALSGAARD
Teoretisk Astrofysik Center, Danmarks Grundforskningsfond, and Institut for Fysik og Astronomi, Aarhus Universitet, DK-8000 C, Denmark
Received 1994 December 1; accepted 1995 April 10

ABSTRACT

We examine the effect of a uniform vertical magnetic field on the modes of an isothermal stratified atmosphere. The present investigation is a continuation of earlier work by Hasan & Christensen-Dalsgaard in which this problem was studied for rigid boundary conditions. In this paper, the earlier results are extended to different sets of boundary conditions. We demonstrate explicitly how these boundary conditions affect the various elementary wave modes present in the atmosphere. In the weak-field limit, an analytic expression for the dispersion relation is derived, which allows the effect of a weak magnetic field on the modes to be studied. We show that, to lowest order in our perturbation expansion, the oscillation spectrum can be analyzed in terms of (*a*) *p*- and *g*-like modes; (*b*) a magnetic Lamb mode; (*c*) magnetic or slow modes; and (*d*) a gravity-Lamb mode. The first three of these were present in the previous analysis for rigid boundaries, whereas the last is a consequence of the vertical gradients of the displacements at the boundaries. We focus our attention on the properties of this mode and show that it is present even in the moderate to strong field case as a magnetogravity-Lamb mode. The recognition and physical interpretation of this mode is a new feature of the present analysis. We also examine the nature of the eigenfrequency curves in the diagnostic (or K-Ω) diagram and find that, similar to the previous analysis, the modes undergo *avoided crossings*. However, the nature of the solutions in the present case is more complicated, especially when triple-mode interactions occur. Furthermore, the connectivity of the curves in the K-Ω diagram can be strongly influenced by the choice of boundary conditions. Our results, though somewhat idealized, find application in the analysis of waves in sunspots. It is conjectured that conditions for the existence of the magnetogravity-Lamb mode may also be satisfied in the subphotospheric layers of the Sun.

Subject headings: MHD — Sun: atmosphere — Sun: magnetic fields — Sun: oscillations

1. INTRODUCTION

In the past 25 years, observations of oscillations with periods in a fairly broad range of frequencies have been reported in magnetic elements of the solar atmosphere (e.g., Beckers & Schulz 1972; Giovanelli, Harvey, & Livingston 1978; Moore & Robin 1985). A study of wave motions can reveal useful information about the nature of magnetic structures. The aim of the present study is to contribute toward developing a theory for such wave motions, also known as magnetoatmospheric oscillations.

The first theoretical study of magnetoatmospheric waves was initiated by Ferraro & Plumpton (1958), where solutions for a stratified isothermal atmosphere with a vertical magnetic field were obtained. This analysis was carried further by Zhugzhda (1979) and Zhugzhda & Dzhalilov (1982 [hereafter ZD], 1984a, b), in which exact solutions were obtained in terms of Meijer functions. Local dispersion relations based on a WKB approach had earlier been used (McLellan & Winterberg 1968; Nagakawa, Priest, & Wellck 1973) to study wave modes in a magnetized stratified atmosphere. However, in order to determine accurately the frequency spectrum, global dispersion relations are needed. These are usually difficult to obtain in terms of analytic expressions, apart from certain limits. The frequency spectrum in the strong-field limit was calculated analytically in the quasi-Alfvénic approximation by Uchida & Sakurai (1975) and numerically by Scheuer & Thomas (1981), Hasan & Abdelatif (1990), Abdelatif (1990), and Wood (1990). Hasan & Christensen-Dalsgaard (1992, hereafter Paper I) extended this analysis to the weak-field limit and obtained an analytic dispersion relation for the wave modes. They examined the effect of a weak field on the normal modes of a stratified isothermal atmosphere and demonstrated that the normal modes of a magnetized atmosphere can be analyzed to lowest order in terms of elementary wave modes of an unmagnetized atmosphere along with purely magnetic modes. Mode coupling was also studied, and it was shown that this coupling becomes particularly important at the locations in the diagnostic diagram where the frequencies of different elementary modes coincide.

In the present paper we extend the previous analysis for different sets of boundary conditions. We attempt to analyze the physical nature of magnetoacoustic gravity (or MAG) oscillations and also to understand the cause for the existence of different types of elementary wave modes in a magnetic isothermal atmosphere subject to different sets of boundary conditions. The results are compared with those for the nonmagnetic case, and the nature of coupling between the elementary wave modes and their properties in the different regions of the diagnostic diagram is analyzed.

The plan of the paper is as follows: in § 2 the basic coupled wave equation for MAG waves is presented for an isothermal stratified atmosphere in a vertical magnetic field. In § 3 we present the dispersion relation for a weak field subject to different sets of

boundary conditions. We examine the behavior of the solution, when different elementary wave mode frequencies come closer. In §§ 4 and 5 numerical results are presented showing the variation of eigenfrequencies with horizontal wavenumbers for the case of a weak field. In § 6 we treat the strong-field case and examine the K-Ω diagram. Finally, a discussion of the results and a comparison with previous studies are taken up in § 7.

2. WAVE EQUATIONS IN A UNIFORM VERTICAL FIELD

We consider an isothermal plane stratified atmosphere, embedded in a uniform vertical magnetic field B, which is unbounded in the horizontal direction. The equations governing MAG modes can be derived by perturbing and linearizing the MHD equations. We assume a Cartesian geometry where z, the vertical coordinate, is measured positive upward, k is the horizontal wavenumber, ω is the frequency, g is the acceleration resulting from gravity, γ is the ratio of specific heats, c_S is the sound speed, and v_A is the Alfvén speed. The sound and Alfvén speeds are defined respectively as

$$c_S = \sqrt{\frac{\gamma p}{\rho}} \quad \text{and} \quad v_A = \frac{B}{\sqrt{4\pi\rho}}, \tag{1}$$

where p is the gas pressure and ρ is the mass density.

We have implicitly assumed that the propagation and motions of the MAG modes are confined to the x-z plane. This involves no loss of generality. Since the equilibrium atmosphere is isothermal, c_S is constant with z, and ρ has the folowing height dependence:

$$\rho = \rho_0 e^{-z/H}, \tag{2}$$

where H is the scale height of the atmosphere and ρ_0 is the mass density at $z = 0$.

In order to obtain a dimensionless wave equation, we introduce three dimensionless parameters

$$K = kH, \tag{3}$$

$$\Omega = \frac{\omega H}{c_S}, \tag{4}$$

and the dimensionless vertical coordinate

$$\theta = \frac{\omega H}{v_A} = \frac{c_S}{v_{A,0}} \Omega e^{-z/(2H)}, \tag{5}$$

where $v_{A,0}$ is the Alfvén speed at $z = 0$. In terms of the variables defined by equations (3)–(5), we have the following equation for MAG waves in a stratified atmosphere (Zhugzhda 1979; see also Paper I):

$$\left\{\theta^4 \frac{d^4}{d\theta^4} + 4\theta^3 \frac{d^3}{d\theta^3} + [1 + 4(\Omega^2 - K^2) + 4\theta^2]\theta^2 \frac{d^2}{d\theta^2} - [1 - 4(\Omega^2 + K^2) - 12\theta^2]\theta \frac{d}{d\theta} + 16\left[\left(\Omega^2 + K^2\left(\frac{\Omega_{BV}^2}{\Omega^2} - 1\right)\right)\theta^2 - \Omega^2 K^2\right]\right\}\xi_x = 0, \tag{6}$$

where $\Omega_{BV}^2 = (\gamma - 1)/\gamma^2$ is the squared Brunt-Väisälä frequency (in dimensionless units). The general solution of equation (6), which can be expressed in terms of Meijer functions (ZD), is given in Appendix B, along with the asymptotic expansions in the weak-field limit.

3. ASYMPTOTIC PROPERTIES OF NORMAL MODES IN THE WEAK-FIELD LIMIT

We examine now the asymptotic properties of waves and normal modes of a stratified atmosphere with a weak magnetic field (corresponding to the limit of small ϵ, where $\epsilon = v_{A,0}/c_S$). The analysis is based on the asymptotic solution developed in Paper I and described in Appendix B; here, however, we consider various different boundary conditions. The analytical results are used in the interpretation of the numerical solutions presented in § 4.

In order to obtain a physical picture of the solution, we consider the upward propagation of a wave, excited from below at $z = 0$, in an isothermal atmosphere. We assume implicitly that the properties of the atmosphere change abruptly at the top boundary, resulting in downward reflection of the waves. The lower boundary condition is chosen to simulate a forcing layer. This permits standing wave solutions. It should be kept in mind that an isothermal atmosphere by itself does not trap modes; however, artificially restricting the boundaries by enforcing boundary conditions may help us to study the physical properties of the modes in a stratified atmosphere with a vertical field.

3.1. *Zero-Gradient Boundary Conditions*

We consider first the case of zero-gradient boundary conditions at the top and bottom of the layer,

$$\frac{d\xi_x}{dz} = \frac{d\xi_z}{dz} = 0 \quad \text{at} \quad z = 0 \quad \text{and} \quad z = d; \tag{7}$$

here d is the height of the top boundary. Substituting equations (B5) and (B6) into equation (7) yields the following dispersion

relation (for details of the derivation, see Appendix B and Paper I):

$$\left(K_z^2+\frac{1}{4}\right)(\Omega^2-K^2)\sin\tilde{\theta}\sin(K_zD)=2\left(K_z^2+\frac{1}{4}\right)\frac{\epsilon}{\Omega}e^{D/4}\left\{K_zK^3\left[\cosh\left(\frac{D}{4}\right)\cos\tilde{\theta}\cos(K_zD)-\cosh\left(\frac{D}{2}\right)\right]\right.$$
$$\left.+\sinh\left(\frac{D}{4}\right)\cos\tilde{\theta}\sin(K_zD)\left[\left(M+\frac{1}{4}\right)(\Omega^2-K^2)-K^3\left(\frac{1}{\gamma}-\frac{1}{2}\right)\right]\right\}+O\left(\frac{\epsilon^2}{\Omega^2}\right), \quad (8)$$

where K_z^2 is given by

$$K_z^2=\Omega^2-K^2\left(1-\frac{\Omega_{\rm BV}^2}{\Omega^2}\right)-\frac{1}{4}; \quad (9)$$

furthermore,

$$M=K^2\frac{\Omega_{\rm BV}^2}{\Omega^2}-\frac{1}{16}, \quad (10)$$

$$\theta_0=\theta(0), \qquad \theta_D=\theta(D), \qquad \tilde{\theta}=2(\theta_0-\theta_D), \quad (11)$$

and $D=d/H$ is the dimensionless height. In Appendix B, the coefficient of the second-order term is also provided.

3.1.1. *The Separate Solutions*

For $\epsilon \ll \Omega$, the dispersion relation, to lowest order in ϵ/Ω, becomes

$$(K_z^2+\tfrac{1}{4})(\Omega^2-K^2)\sin\tilde{\theta}\sin(K_zD)=0. \quad (12)$$

Equation (12) leads to the following separate dispersion relations:

$$\sin(K_zD)=0, \quad (13a)$$

$$\Omega=K, \quad (13b)$$

$$\sin\tilde{\theta}=0, \quad (13c)$$

$$K_z^2+\tfrac{1}{4}=0. \quad (13d)$$

The solutions corresponding to equations (13a)–(13c) have already been discussed in Paper I. The solutions of equations (13a) and (13b) correspond to the usual p- and g-modes in an unmagnetized atmosphere and the Lamb mode, respectively, whereas equation (13c) yields the magnetic (or m-) modes, with frequencies

$$\Omega_m=\frac{\epsilon l\pi}{2s} \qquad (l=1, 2, \ldots), \quad (14)$$

where $s=1-e^{-D/2}$.

Now we turn our attention to the solution of equation (13d) which is a new feature of the present analysis. Using equations (9) and (13d), we obtain

$$\Omega^4-\Omega^2K^2+K^2\Omega_{\rm BV}^2=0. \quad (15)$$

This equation has the solution

$$\Omega^2=\frac{1}{2}K^2\left[1\pm\left(1-4\frac{\Omega_{\rm BV}^2}{K^2}\right)^{1/2}\right]; \quad (16)$$

thus, a real frequency is found only for $K \geq 2\Omega_{\rm BV}$. The solution resembles a gravity mode on the lower branch and a Lamb mode on the upper branch. In order to see this, consider the limit $K \to \infty$. The smaller solution in equation (16) has the limit $\Omega \simeq \Omega_{\rm BV}$, which is the dispersion relation for a g-mode for large K; the larger solution has the limit $\Omega \simeq K$ for large K, which shows that the mode behaves like a pure Lamb wave. Therefore, the mode will henceforth be referred to as a *gravity-Lamb* (or *gL*-) mode. More details about the properties of this mode and its interaction with other modes in the K-Ω diagram will be considered in § 5. This mode was not found in Paper I, where rigid boundary conditions were used. It exists even in a nonmagnetic atmosphere, as can easily be seen by looking at the solution for the vertical displacement, which is

$$\xi_z=e^{z/2H}[A\sin(K_zZ)+B\cos(K_zZ)], \quad (17)$$

where A and B are constants. If we apply the boundary conditions in equation (7), we obtain the exact dispersion relation

$$(K_z^2+\tfrac{1}{4})\sin(K_zD)=0, \quad (18)$$

yielding again equation (13d). From equation (B10), we find that in the presence of a weak magnetic field the dispersion relation for this mode is not modified, at least to $O(\epsilon^2)$. In fact, as we shall see in § 6, this mode is present even when there is a strong magnetic field, though with a modified dispersion relation.

The frequencies of the magnetic m-modes (eq. [14]) are independent of K, whereas the frequencies of the Lamb mode increase linearly with K. The p- and g-mode frequencies, as determined by equations (13a) and (13c), also increase with K; thus, it is evident that for some value of K the p-, g-, and Lamb mode frequencies will cross the pure m-mode frequencies. However, in the vicinity of such a crossing point the right-hand side of equation (8) can no longer be neglected. It has the effect of turning the crossing of the frequencies into *avoided crossings*, as was also discussed in Paper I. In the following sections we consider the behavior in the vicinity of such avoided crossings.

3.1.2. *Avoided Crossings between the Lamb Mode and the m-Modes*

We consider first crossings between the Lamb mode and the magnetic modes. In the vicinity of the unmodified Lamb mode, with $\Omega = K_z$, K_z becomes imaginary. Hence, in equation (8) we replace K_z with $\tilde{K}_z = |K_z|$, sin $(\tilde{K}_z D)$ by sinh $(\tilde{K}_z D)$ and cos $(K_z D)$ by cosh $(\tilde{K}_z D)$. Crossing of the pure modes occurs at $K = K_l = \Omega_m$, where Ω_m is given by equation (14); at this point equation (9) shows that $\tilde{K}_z = 1/\gamma - \frac{1}{2}$. To analyze the behavior of the full dispersion relation (8) around this point, we let

$$K = K_l + \delta K\,, \qquad \Omega = \Omega_m + \delta\Omega\,, \tag{19}$$

where δK and $\delta\Omega$ are regarded as small quantities. We expand $\tilde{\theta}$ to obtain $\tilde{\theta} = l\pi + 2s/\epsilon\,\delta\Omega$. Replacing $\tilde{K}_z$ and the right-hand side by the values at the crossing, we obtain the approximate dispersion relation

$$\begin{aligned}(-1)^l \frac{4s}{\epsilon}(\Omega_m\,\delta\Omega - K_l\,\delta K)\delta\Omega \sinh\left[\left(\frac{1}{\gamma}-\frac{1}{2}\right)D\right] &= 2\frac{\epsilon}{\Omega_m} e^{D/4}\left\{\left(\frac{1}{\gamma}-\frac{1}{2}\right)K_l^3\left[(-1)^l \cosh\left(\frac{D}{4}\right)\cosh\left[\left(\frac{1}{\gamma}-\frac{1}{2}\right)D\right] - \cosh\left(\frac{D}{2}\right)\right]\right.\\ &\quad \left. -(-1)^l \sinh\left(\frac{D}{4}\right)\sinh\left[\left(\frac{1}{\gamma}-\frac{1}{2}\right)D\right]K_l^3\left(\frac{1}{\gamma}-\frac{1}{2}\right)\right\}\\ &= (-1)^l \frac{2\epsilon}{\Omega_m} e^{D/4}\left(\frac{1}{\gamma}-\frac{1}{2}\right)K_l^3\left\{\cosh\left[\left(\frac{3}{4}-\frac{1}{\gamma}\right)D\right] - (-1)^l \cosh\left(\frac{D}{2}\right)\right\}\,,\end{aligned} \tag{20}$$

or

$$(\delta\Omega^2 - \delta K\,\delta\Omega)\sinh\left[\left(\frac{1}{\gamma}-\frac{1}{2}\right)D\right] = \frac{\epsilon^2}{2s} e^{D/4}\left(\frac{1}{\gamma}-\frac{1}{2}\right)K_l\left\{\cosh\left[\left(\frac{3}{4}-\frac{1}{\gamma}\right)D\right] - (-1)^l \cosh\left(\frac{D}{2}\right)\right\}. \tag{21}$$

This gives a quadratic equation for $\delta\Omega$, which may be written as

$$\delta\Omega^2 - \delta K\,\delta\Omega - \tfrac{1}{4}\delta\Omega_{\min}^2 = 0\,, \tag{22}$$

with the solution

$$\delta\Omega = \tfrac{1}{2}\,\delta K \pm \tfrac{1}{2}(\delta K^2 + \delta\Omega_{\min}^2)^{1/2}\,. \tag{23}$$

Here

$$\delta\Omega_{\min}^2 = 16\frac{\eta^2}{\pi^2} K_l \frac{\sinh\,(D/4)}{\sinh\,[(1/\gamma - 1/2)D]}\left(\frac{1}{\gamma}-\frac{1}{2}\right)\left\{\cosh\left[\left(\frac{3}{4}-\frac{1}{\gamma}\right)D\right] - (-1)^l \cosh\left(\frac{D}{2}\right)\right\}, \tag{24}$$

where $\eta = \epsilon\pi/2s$ is the separation between the frequencies of adjacent magnetic modes.

In the case of rigid boundaries (Paper I) a similar expression was found, where $\delta\Omega_{\min}^2$ was nonnegative for all values of l (see eq. [46] of Paper I); hence, in that case the roots were always real. In contrast, for the solution given by equations (23) and (24) $\delta\Omega_{\min}^2$ is negative for even values of l. Hence, in the present case of vanishing gradients of the displacements at the boundaries, we obtain pairs of complex conjugate roots for even values of l when K is within the range $\pm|\,\delta\Omega_{\min}\,|$ of the location of the crossing of the pure modes. The consequences of this for the global behavior of the eigenfrequencies are discussed in § 4, based on numerical solutions of the oscillation equations.

We now consider the minimum frequency separation $\delta\Omega_{\min}^{(+)}/\eta$ in an avoided crossing between the Lamb mode and a magnetic mode of odd values of l, shown in Figure 1 as a function of K for different D. Unlike the zero-displacement case (see Fig. 4*b* of Paper I), one finds that in this case the minimum separation depends on K. Clearly, values of $\delta\Omega_{\min}^{(+)}/\eta$ exceeding unity indicate a breakdown of the asymptotic description, and this occurs at smaller values of K in the case of zero-gradient boundaries. The dashed lines similarly show $|\,\delta\Omega_{\min}^{(-)}/\eta\,|$ for even values of l, corresponding to the range of K around the avoided crossing for which there are complex conjugate roots; thus, $2\,|\,\delta\Omega_{\min}^{(-)}\,|$ gives the minimum separation in K between the eigencurves at such an avoided crossing.

3.1.3. *Avoided Crossings between p- or g-Modes and m-Modes*

We now consider a crossing between a p- or g-mode of order n, characterized by $K_z D = n\pi$, and a magnetic mode of order l with frequency $\Omega_m = \epsilon\pi l/2s$. We know from equation (9) that the crossing will take place at the point (K_{nl}, Ω_m) in the (K, Ω) diagram where

$$\frac{n^2\pi^2}{D^2} = \Omega_m^2 - K_{\rm nl}^2\left(1 - \frac{\Omega_{\rm BV}^2}{\Omega_m^2}\right) - \frac{1}{4}\,. \tag{25}$$

As before, we let

$$K = K_{\rm nl} + \delta K\,, \qquad \Omega = \Omega_m + \delta\Omega\,. \tag{26}$$

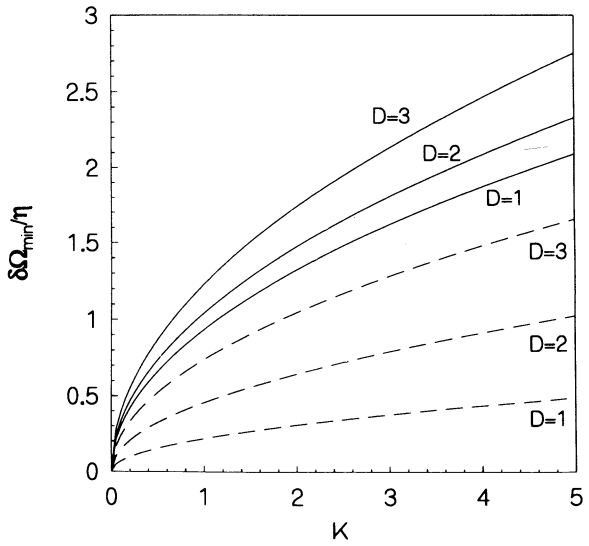

FIG. 1.—Asymptotic values for the minimum separation $\delta\Omega_{min}$, in units of η, between adjacent avoided crossings between the Lamb mode and magnetic modes, as a function of K, for $\epsilon = 0.01$ and $\gamma = 5/3$. Solid lines show $\delta\Omega^{(+)}_{min}/\eta$ for $D = 1$, 2, and 3 for odd values of l, whereas dashed lines show $|\delta\Omega^{(-)}_{min}/\eta|$ for even values of l, for the same values of D.

Expanding K_z, we obtain

$$K_z \simeq \frac{n\pi}{D} - \frac{DK_{nl}}{n\pi}\left(1 - \frac{\Omega_{BV}^2}{\Omega_m^2}\right)\delta K + \frac{D\Omega_m}{n\pi}\left(1 - K_{nl}^2\frac{\Omega_{BV}^2}{\Omega_m^4}\right)\delta\Omega\,. \tag{27}$$

The expansion of $\tilde{\theta}$ was already given in § 3.1.2. We substitute these expansions into the left-hand side of equation (8), while the right-hand side and the factor $\Omega^2 - K^2$ are evaluated at (K_{nl}, Ω_m). This leads to

$$(-1)^{n+l}\frac{2s}{\epsilon}(\Omega_m^2 - K_{nl}^2)\frac{D^2}{n\pi}\left[\left(1 - K_{nl}^2\frac{\Omega_{BV}^2}{\Omega_m^4}\right)\Omega_m\,\delta\Omega - \left(1 - \frac{\Omega_{BV}^2}{\Omega_m^2}\right)K_{nl}\,\delta K\right]\delta\Omega = \frac{\epsilon}{\Omega_m}e^{D/4}\frac{2n\pi}{D}K_{nl}^3\left[(-1)^{n+l}\cosh\left(\frac{D}{4}\right) - \cosh\left(\frac{D}{2}\right)\right], \tag{28}$$

which can be further simplified to

$$\delta\Omega^2 - \frac{K_{nl}\Omega_m(\Omega_m^2 - \Omega_{BV}^2)}{\Omega_m^4 - K_{nl}^2\Omega_{BV}^2}\,\delta K\,\delta\Omega - \frac{\epsilon^2\pi^2n^2}{D^3s}\frac{K_{nl}^3[\cosh(D/4) - (-1)^{n+l}\cosh(D/2)]}{(\Omega_m^2 - K_{nl}^2)(\Omega_m^4 - K_{nl}^2\Omega_{BV}^2)} = 0\,. \tag{29}$$

Equation (29) provides a quadratic equation for $\delta\Omega$ as a function of δK. For $\delta K = 0$, the minimum separation between two branches can be obtained from equation (29) as

$$\delta\Omega_{min}^2 = \frac{4s\eta^2n^2}{D^3}\frac{K_{nl}^3[\cosh(D/4) - (-1)^{n+l}\cosh(D/2)]}{(\Omega_m^2 - K_{nl}^2)(\Omega_m^4 - K_{nl}^2\Omega_{BV}^2)}\,. \tag{30}$$

The behavior near the avoided crossing depends crucially on $n + l$. When $n + l$ is odd, we obtain a normal avoided crossing in Ω. On the other hand, $\delta\Omega_{min}^2$ is negative for even values of $n + l$, so that real solutions are again absent near the avoided crossings. We also note that $\delta\Omega_{min}$ increases with K approximately as $K_{nl}^{3/2}$, i.e., more rapidly than for the avoided crossings between the Lamb mode and the magnetic modes (see eq. [24]).

3.1.4. *Avoided Crossings with the Gravity-Lamb Mode*

According to equation (B10), $K_z^2 + \frac{1}{4}$ is a factor to all terms in the dispersion relation, up to and including the term of order ϵ^2. Thus, to this order, there is exact crossing between the gL-mode and the remaining modes, and an analysis similar to the one carried out in §§ 3.1.2 and 3.1.3 is not possible. In § 5.1 we show, from numerical computations, that the actual behavior in the vicinity of the crossing points does indeed lead to avoided crossings with regions in K with no real solutions, the minimum separation scaling roughly as ϵ^2. This suggests that the exact factorization ceases to hold in the term of order ϵ^3 in equation (B10).

3.2. *Mixed Boundary Conditions*

To analyze the effects of boundary conditions on the various elementary wave models, we have chosen different combinations of conditions on the displacements at the boundaries. Specifically, we examine now the behavior of the normal modes for the following boundary conditions:

$$\xi_x = \xi_z = 0 \qquad \text{at} \qquad z = 0\,, \tag{31a}$$

and

$$\frac{d\xi_x}{dz} = \frac{d\xi_z}{dz} = 0 \qquad \text{at} \qquad z = d\,. \tag{31b}$$

This choice corresponds to a node at the base and an antinode at the top boundary. As before, the asymptotic dispersion relation can be obtained by substituting equations (B3) and (B4) into equation (31a) and equations (B5) and (B6) into equation (31b); here we consider only the lowest order terms, obtaining

$$[\sin (K_z D) + 2K_z \cos (K_z D)](\Omega^2 - K^2) \cos \tilde{\theta} = 0\,. \tag{32}$$

As before, to this order the dispersion relation has separated solutions. We obtain the following separate dispersion relations:

$$K_z + \tfrac{1}{2} \tan (K_z D) = 0\,, \tag{33a}$$

$$\Omega = K\,, \tag{33b}$$

$$\cos \tilde{\theta} = 0\,. \tag{33c}$$

The solutions of equations (33b) and (33c) correspond to the Lamb and magnetic modes, discussed earlier. The Lamb mode is unaffected by the change in boundary conditions, while for the magnetic modes the frequencies are given by

$$\Omega_m = \frac{\epsilon\pi}{2s}\left(l + \frac{1}{2}\right) \qquad (l = 0, 1, 2, \ldots)\,; \tag{34}$$

thus, they are shifted by an amount $\epsilon\pi/4s$ in the diagnostic diagram with respect to the m-modes calculated for the previous sets of boundary conditions treated in § 3.1 and in Paper I. However, the frequency separation between adjacent modes is the same as before.

We now return to the solution of equation (33a), which represents the modified form of the p- and g-mode dispersion relation. In fact, by applying the boundary conditions (31a)–(31b) to the solution ξ_z for an isothermal nonmagnetic atmosphere given by equation (17), we get the exact dispersion relation

$$\sin (K_z D) + 2K_z \cos (K_z D) = 0\,, \tag{35}$$

which is identical to equation (33a). For large mode order n, the solution can be approximated as

$$K_z D \simeq (n + \tfrac{1}{2})\pi\,. \tag{36}$$

This expansion yields the usual p- and g-modes with a frequency shift, as compared to Paper I and the previous case (§ 3.1), as a result of the additional term of $\pi/2$ on the right-hand side of equation (36).

The general result of this analysis is, therefore, that the overall frequency spectrum of the p- and g-modes, magnetic modes, and the Lamb mode for a magnetic atmosphere (apart from a possible constant frequency shift) is insensitive to the precise nature of the boundary conditions.

We have also considered the normal modes for yet another set of boundary conditions, namely,

$$\xi_x = \xi_z = 0 \qquad \text{at} \qquad z = d\,, \tag{37a}$$

and

$$\frac{d\xi_x}{dz} = \frac{d\xi_z}{dz} = 0 \qquad \text{at} \qquad z = 0\,. \tag{37b}$$

The results are the same as for the above case, because of symmetry. One can check this easily by using equation (17) for an isothermal nonmagnetic atmosphere.

In principle, the coupling between the separate solutions at points where they cross could be analyzed by including the term $O(\epsilon)$ in the dispersion relation (32). However, as discussed in § 4.3 below, we have found that the behavior of the numerical results deviates strongly from the resulting expression. We shall not pursue this further here.

4. K-Ω DIAGRAMS FOR A WEAK FIELD

We consider now numerical results for the weak-field case. The solutions were computed by solving equation (6) (formulated as a system of first-order differential equations) with the fourth-order Newton-Raphson-Kantorovich scheme (Cash & Moore 1980) which was also used in Paper I. We consider first the case of using the zero-gradient boundary conditions in equations (7a)–(7b). Figure 2*a* depicts the resulting variation of frequency with horizontal wavenumber, for $\epsilon = 0.01$, $\gamma = 5/3$ and $D = 1$ (this default case is used unless otherwise noted). The long dashed line corresponds to the Lamb solution $\Omega = K$, and the short dashed lines correspond to the gravity modes g_1, g_2 in a nonmagnetic atmosphere. The solid and dotted lines, respectively, correspond to the numerical solution of equation (6) and the roots of the analytical dispersion relation (eq. [B10]).

The default choice $D = 1$ for the vertical extent of the cavity may appear to be somewhat idealized and not relevant to photospheric flux tubes. This choice is basically made to allow us to use the asymptotic analysis for a weak field over the entire

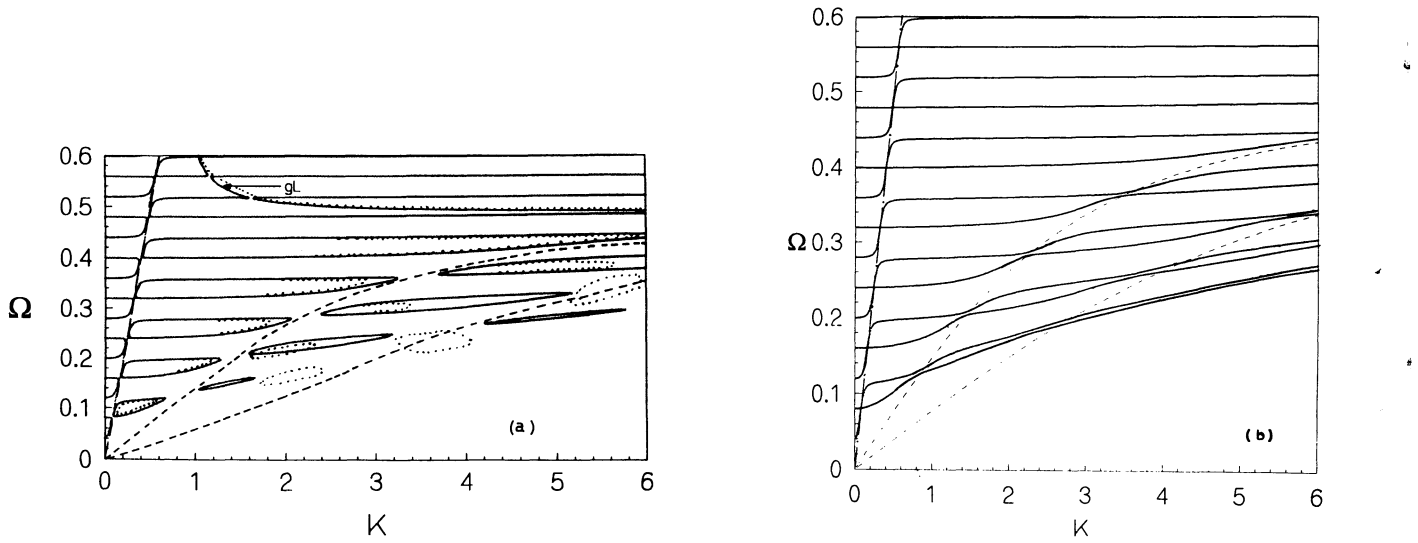

FIG. 2.—Variation of Ω with K in an isothermal atmosphere using the default values $\epsilon = 0.01$, $D = 1$, and $\gamma = 5/3$. Long-dashed curve represents the Lamb solution $\Omega = K$, and short-dashed curves correspond to the g_1- and g_2-modes in a nonmagnetic atmosphere. (*a*) Results for zero-gradient boundary conditions; solid lines correspond to the numerical solution of eq. (6), and dotted lines correspond to the solution of the dispersion relation (B10). (*b*) Results for rigid boundary conditions; solid lines correspond to the numerical solution of eq. (6).

extent of the atmosphere. The asymptotic analysis proves to be an extremely valuable tool for understanding the modal structure and permits us to understand the numerical results much better. By gradually increasing D, it is possible to see how the modal structure is modified and also to classify the modes.

We compare first the numerical results with those obtained by solving the analytical dispersion relation (eq. [B10]). For small values of K (roughly when $K < 1$), the agreement between the two sets of curves is very good. However, as K increases the two sets of solutions begin to differ, with the largest discrepancy for small values of Ω. The reason for this behavior has already been discussed in Paper I: it is essentially a result of the breakdown of the asymptotic expansion for large K, such that $K^2 \gtrsim \Omega^3 v_A/c_S$.

It is interesting to compare the results shown in Figure 2*a* with those obtained in Paper I using rigid boundary conditions. The latter are shown in Figure 2*b*. The most important qualitative difference between the two sets of calculations is in the appearance of the gravity-Lamb mode, labeled *gL*. This mode corresponds to the solution of equation (13d). The remaining solutions for $\Omega < 0.6$ (the region shown in Figs. 2*a* and 2*b*) consist of magnetic or *m*-modes, which interact with the Lamb mode (for $\Omega \simeq K$) or with the *g*-modes when equation (13a) is satisfied; as pointed out in Paper I, the frequency is restricted to be above the frequency of the m_1-mode.

Comparison of Figures 2*a* and 2*b* shows that with the exception of the *gL*-mode the solutions are very similar for the two sets of boundary conditions apart from the vicinity of the avoided crossings. We turn now to an analysis of these, based on the asymptotic results obtained in § 3. The interactions between the *gL*-mode and the remaining modes are discussed in § 5.

4.1. *Avoided Crossings between the Lamb Mode and the m-Modes*

Figure 3 shows an enlargement of a portion of Figure 2*a*, showing the interaction of the lowest order *m*-modes with the Lamb mode. The modes corresponding to even-order *m*-modes at $K = 0$ do not have real solutions near the intersection points. On the other hand, as an odd *m*-mode approaches the $\Omega = K$ curve it acquires the character of a Lamb mode and avoids crossing it by merging with the next higher order even mode. Thus, the odd- and even-order magnetic modes behave differently as they approach the $\Omega = K$ curve; this is in accordance with the asymptotic expressions (23) and (24). The odd *m*-modes undergo a mode transformation to a Lamb mode, but since there is no real solution for the even-ordered *m*-modes near the avoided crossings, they cannot cross the intersection point and as a result merge with the modified Lamb mode. These merged modes reappear again at some distance away from the avoided crossing and separate out as two independent magnetic modes. Thus, the asymptotic analysis explains the difference in the connectivity of the eigencurves near the avoided crossings for even and odd values of l. Note that this result is entirely different from the case of rigid boundaries (considered in Paper I), where $\delta\Omega_{\min}$ is always real for all values of l. Consequently, in that case, for all l the nature of the solutions near the intersection points follows the pattern of the odd solutions found for zero-gradient boundary conditions.

4.2. *Avoided Crossings between the m-Modes and the g- and p-Modes*

Figure 4*a* shows the interaction between *g*- and *m*-modes, assuming default values of the parameters. We first consider the m_1-mode. As K increases, this mode acquires the character of a g_1-mode. In accordance with the asymptotic description in equation (30), the nature of the solution near the intersection point, similar to the previous section, is one where this mode merges with m_2. To the right of the intersection point, there are two branches: the lower branch is a modified m_2-mode, whereas the upper is a modified g_1-mode. The latter undergoes an avoided crossing with the magnetic mode m_3, but this time the interaction is different due to the fact that we have an odd *m*-mode. This phenomenon is repeated again when the next odd magnetic mode (m_3), which behaves like a

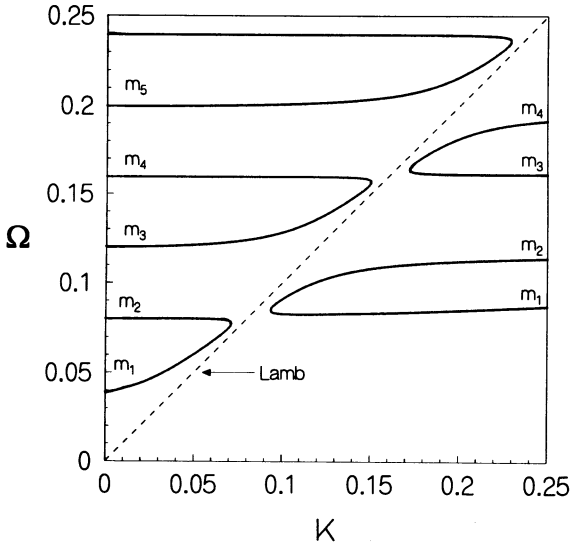

FIG. 3.—Variation of Ω with K in an isothermal atmosphere using the default values $\epsilon = 0.01$, $D = 1$, and $\gamma = 5/3$. Short-dashed curve represents the Lamb solution $\Omega = K$, and solid line corresponds to the numerical solution of eq. (6) with zero-gradient boundary conditions. Magnetic modes have been labeled as m_l ($l = 1, 2, \ldots$).

gravity mode, approaches the m_4-mode. Regarding the two branches on the right of the intersection point, we find that they merge again, possibly due to the influence of the g_2-mode.

At higher values of K the validity of the asymptotic expressions is dubious. However, the qualitative nature of the avoided crossings is similar, leading to the formation of extended "islands" in the K-Ω diagram (see Fig. 2*a*). The location of these islands coincides closely with the almost parallel eigencurves found in the case of zero-displacement boundary conditions (see Fig. 2*b*).

The interaction between the p_1-mode and higher order magnetic modes is depicted in Figure 4*b*. The first avoided crossing (in the lower half of Fig. 4*b*) between the p_1-mode and an odd-order mode (labeled as m_0) leads to a merger in accordance with equation (30), since $n + l$ is even. When these two modes reappear away from the intersection point, they separate into an m-mode and a p_1-mode. When the p_1-mode comes closer to the next even-order m-mode, it undergoes a mode transformation in the form of an ordinary avoided crossing, the p_1- and the m-mode exchanging character. Furthermore, the alternation between the narrow (in K) and wide (in Ω) separations for even and odd $n + l$ is evident here. Thus, the asymptotic analysis enables us to understand the alternate behavior of the magnetic modes, which leads to merging of nearest neighbor eigencurves around an avoided crossing accompanied by mode transformation.

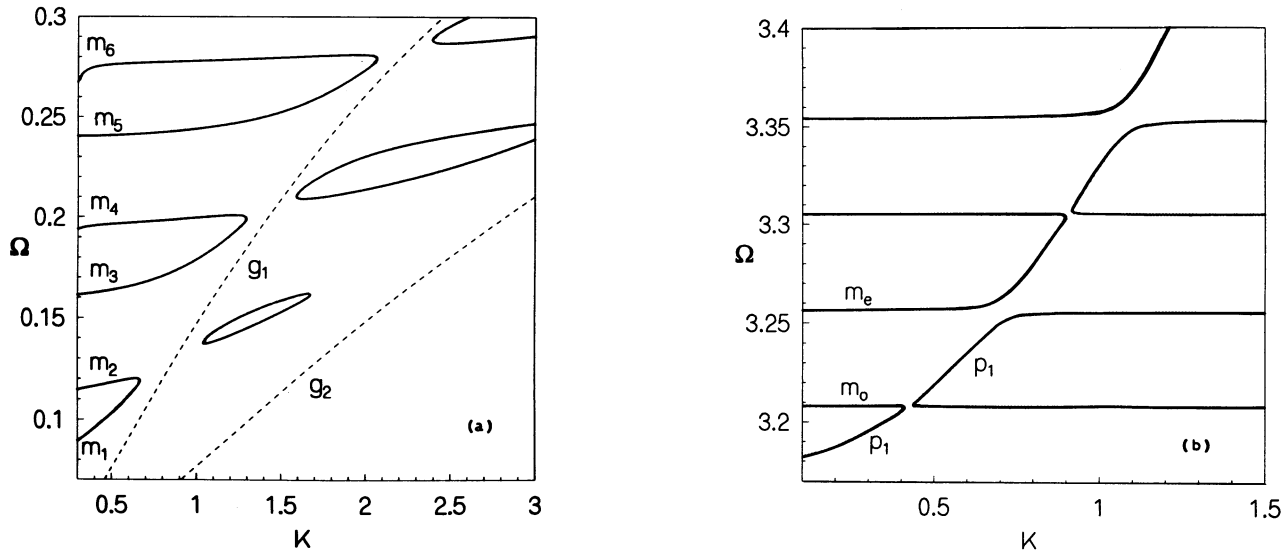

FIG. 4.—Expanded regions of the diagnostic diagram for the default parameters. Solid lines show numerical solutions using zero-gradient boundary conditions. (*a*) Region of interaction between g- and m-type solutions. Solid curves correspond to the magnetic modes and have been labeled as m_l ($l = 1, 2, \ldots$), and dashed curves (labeled as g_1, g_2) show frequencies of g-modes in the field-free case. (*b*) Region of interaction between p- and m-type solutions. Odd- and even-ordered magnetic modes are denoted as m_o and m_e, respectively. The m-modes have orders between 80 and 83.

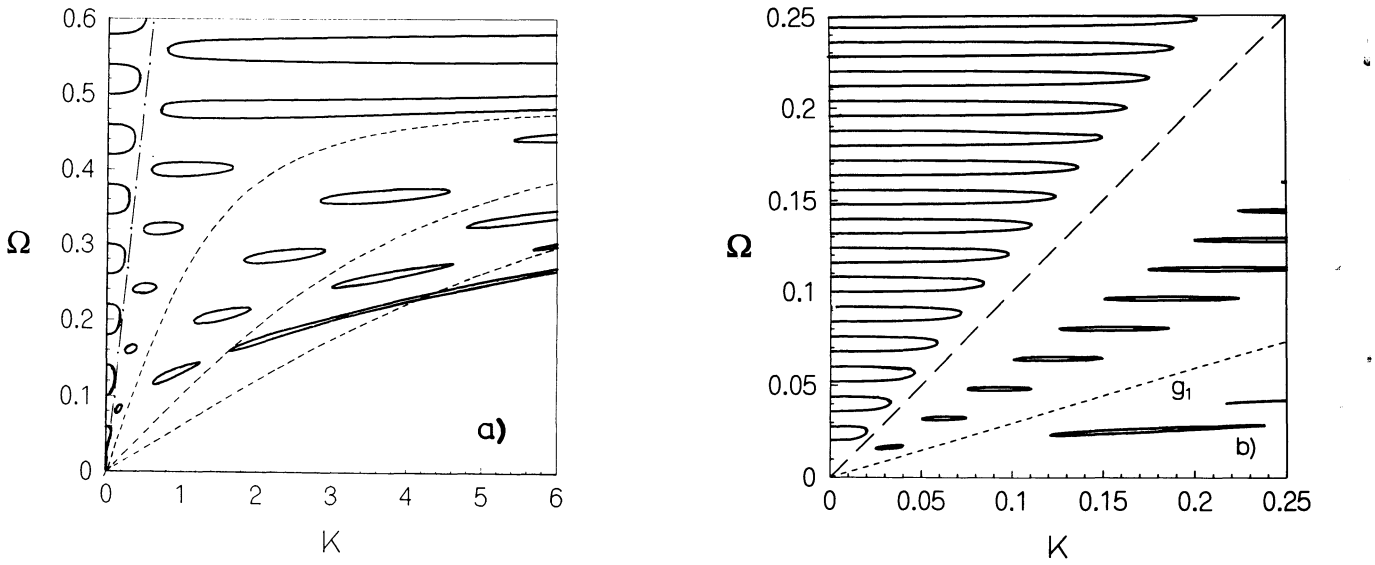

FIG. 5.—Variation of Ω with K in an isothermal atmosphere using the default values $D = 1$ and $\gamma = 5/3$ and the mixed boundary conditions of eqs. (31a) and (31b). Long-dashed curve represents the Lamb solution $\Omega = K$, and short-dashed curves correspond to the g_1-, g_2-, and g_3-modes in a nonmagnetic atmosphere. The following values of ϵ are shown: (*a*) $\epsilon = 0.01$; (*b*) $\epsilon = 0.002$.

4.3. *Mixed Boundary Conditions*

Figure 5*a* shows a K-Ω diagram for mixed boundary conditions (eqs. [31a]–[31b]), using the default parameters. The solid lines show the numerically computed frequencies for this case, whereas the long-dashed and short-dashed lines show the Lamb mode and the lowest order g-modes, respectively. A close inspection shows that the frequencies of the magnetic modes have in fact been shifted by half the frequency separation, as predicted by equation (34). However, the most striking difference from the previous cases is in the behavior at the avoided crossings: although formally these are topologically equivalent to those in Figure 2*b*, alternating between avoidance in Ω and avoidance in K, the separation is now so large as to leave an extended mode-free region surrounding the location of the Lamb mode, with similar regions surrounding the low-order g-modes.

This behavior is particularly striking in Figure 5*b*, which shows the region of low K for $\epsilon = 0.002$, but otherwise using the default parameters. Here the density of magnetic modes is so high that the regions of avoidance are clearly delineated. We have found from the numerical solutions that these regions are essentially independent of the value of ϵ, for small ϵ. This behavior is qualitatively different from what is obtained for zero-displacement or zero-gradient boundary conditions. In particular, we note from equations (24) and (30) that in the latter case $|\delta\Omega_{\rm min}| \propto \epsilon$ at a given point (K, Ω) in the diagnostic diagram. However, for mixed boundary conditions it appears that the minimum separation at avoided crossings is much larger than the separation between adjacent magnetic modes, thus invalidating the simple asymptotic description. We hope to return to this point in a future publication.

We have also computed numerical solutions for the boundary conditions (37a) and (37b). As argued in § 3.2, the separate solutions are the same as in the case considered in Figure 5; however, the behavior at the avoided crossings is even more extreme, leading to an apparent near-suppression of the modes to the right of the Lamb line $\Omega = K$ at frequencies below $\Omega \simeq 0.5$. This case deserves closer scrutiny.

5. PROPERTIES OF THE GRAVITY-LAMB MODE

The gravity-Lamb mode is a new feature of the solution for the zero-gradient boundary conditions. Its interactions with the other modes lead to a number of intricate phenomena, some of which are apparently related to the fact that more than two modes may be involved in a given interaction. Here we examine these interactions in some detail.

5.1. *Avoided Crossings between the Gravity-Lamb Mode and the Magnetic Modes*

The asymptotic analysis in § 3.1 left some uncertainty about the interaction between the gL- and the m-modes in the weak-field limit. To investigate this interaction by means of numerical calculations, Figure 6 shows results for avoided crossings near $\Omega = 0.8$, for $D = 1$, $\gamma = 5/3$, and $\epsilon = 0.01$, 0.02, 0.05, and 0.1. It is evident that the crossings are indeed avoided, leaving regions in K corresponding to complex solutions for Ω. Also, the minimum separation $\delta K_{\rm min}$ in K is extremely small for small ϵ: the numerical results can be approximated quite accurately by $\delta K_{\rm min} \simeq 4.5\epsilon^2$. On the scale of Figure 2, this behavior is evidently entirely invisible.

5.2. *Effect of the Gravity-Lamb Mode on Avoided Crossings between Pure Lamb and Magnetic Modes*

Figure 6 illustrates the interaction between a magnetic mode and what might be considered the pure gravity-Lamb mode. However, the frequency separation between the latter and the ordinary Lamb mode is comparable with, or smaller than, the separation in the avoided crossing for $\epsilon = 0.1$. This suggests that all three modes must be taken into account when studying the interaction. We have not attempted an asymptotic analysis of this very complex case; however, the numerical results provide an indication of the phenomena that it gives rise to.

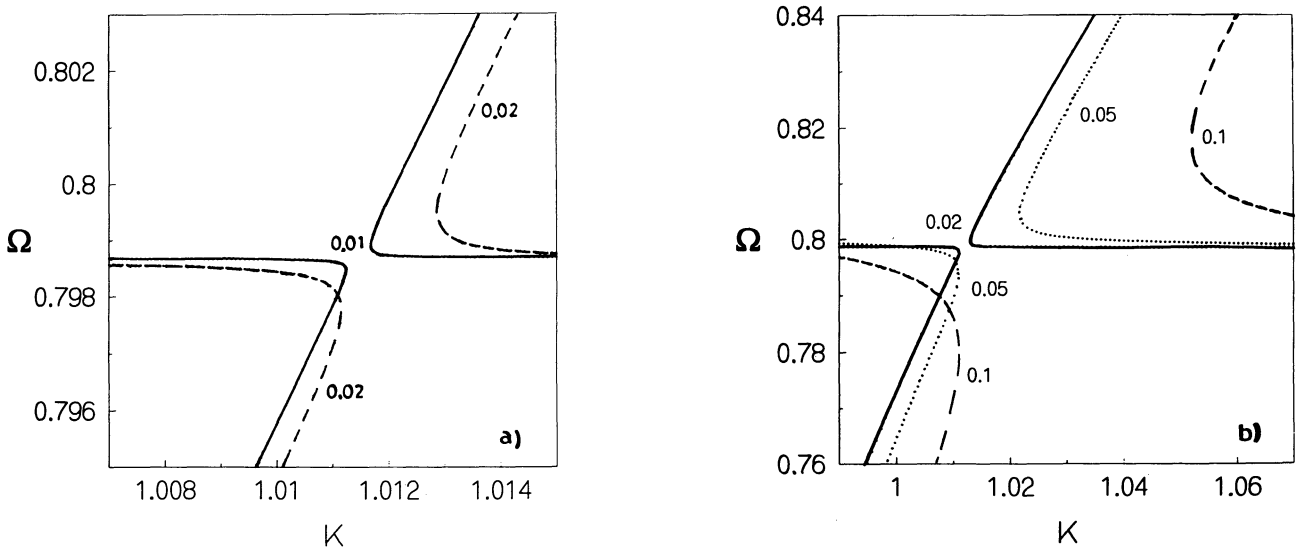

FIG. 6.—Avoided crossings between the gravity-Lamb mode and a magnetic mode, using the zero-gradient boundary conditions of eq. (7), for $D = 1$, $\gamma = 5/3$, and different values of ϵ, as indicated in the figure. (*a*) Solid line is for $\epsilon = 0.01$, and dashed line is for $\epsilon = 0.02$. (*b*) Solid line is for $\epsilon = 0.02$, dotted line is for $\epsilon = 0.05$, and dashed line is for $\epsilon = 0.1$.

As a reference, we first recall briefly the behavior observed in Paper I for rigid boundary conditions. Figure 7*a* shows the avoided crossings between the Lamb mode and magnetic modes for $\epsilon = 0.1$. In the limit $K \to 0$, we denote the magnetic modes m_l ($l = 1, 2, \ldots$). The Lamb mode is represented by the dashed line. The main feature, which has already been pointed out in Paper I, is that successive magnetic modes undergo avoided crossings as a result of one of the modes becoming transformed into a Lamb mode, which then undergoes avoided crossings with the next higher order magnetic mode. This behavior can now be compared with Figure 7*b*, for zero-gradient boundary conditions in equation (7), but otherwise using the same parameters as for Figure 7*a*. In the limit $K \to 0$, and for K substantially higher than the value corresponding to the Lamb mode, the frequencies of the magnetic modes appear at approximately the same locations in the diagnostic diagram as in Figure 7*a*. However, in Figure 7*b* we note the appearance of the gravity-Lamb mode. Also, the mode coupling is much more complicated than before. This can be illustrated by considering in some detail the interactions near the intersection point marked by a cross in Figure 7*b*. As K increases, the m_1-mode begins to acquire the character of a magnetic Lamb mode as before, but as it approaches the intersection point, the two magnetic modes join up. This is equivalent to the behavior observed in Figure 3 for smaller ϵ. However, in the present case the magnetic modes emerging to the right of the interaction immediately encounter the gravity-Lamb mode. This leads to a new pair of avoided crossings, the lower of which was shown in more detail in Figure 6*a*. Only after this additional interaction does the pair of magnetic

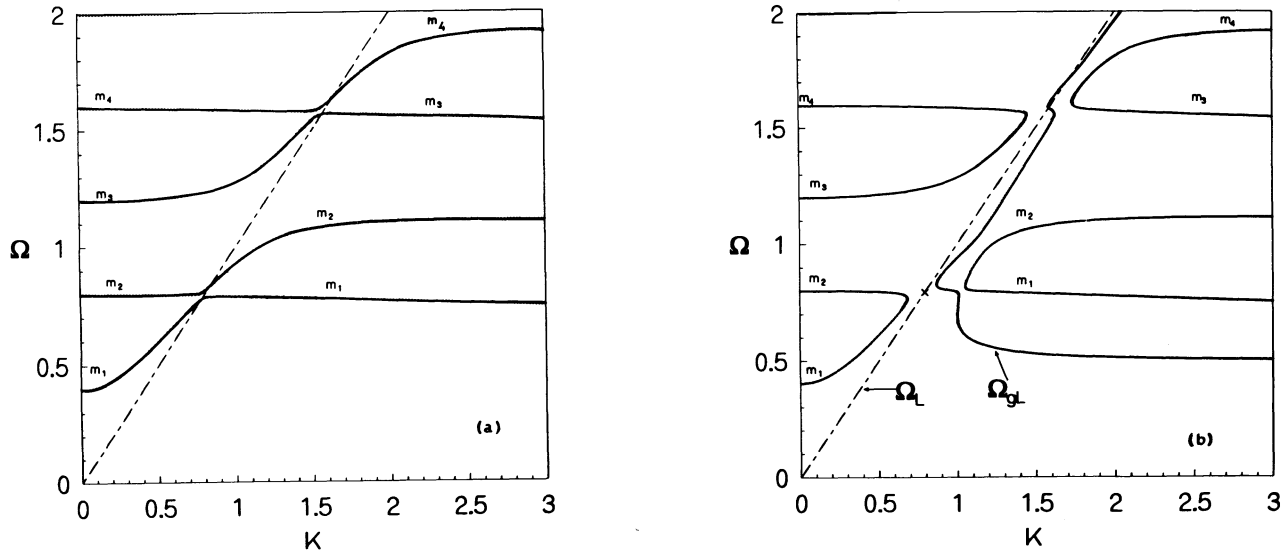

FIG. 7.—Region in the diagnostic diagram, for $\epsilon = 0.1$, where there are magnetic and Lamb-type solutions. Dashed curve corresponds to the pure Lamb solution $\Omega = K$. (*a*) Results for zero-displacement boundary conditions; solid curves show magnetic modes with orders 1–4. (*b*) Results for zero-gradient boundary conditions; the pure Lamb mode ($\Omega = K$) has been shown with a dashed line, and the gravity-Lamb mode frequency (given by eq. [15] has been labeled as Ω_{gL}, whereas the other solid curves correspond to the magnetic modes of order 1–4.

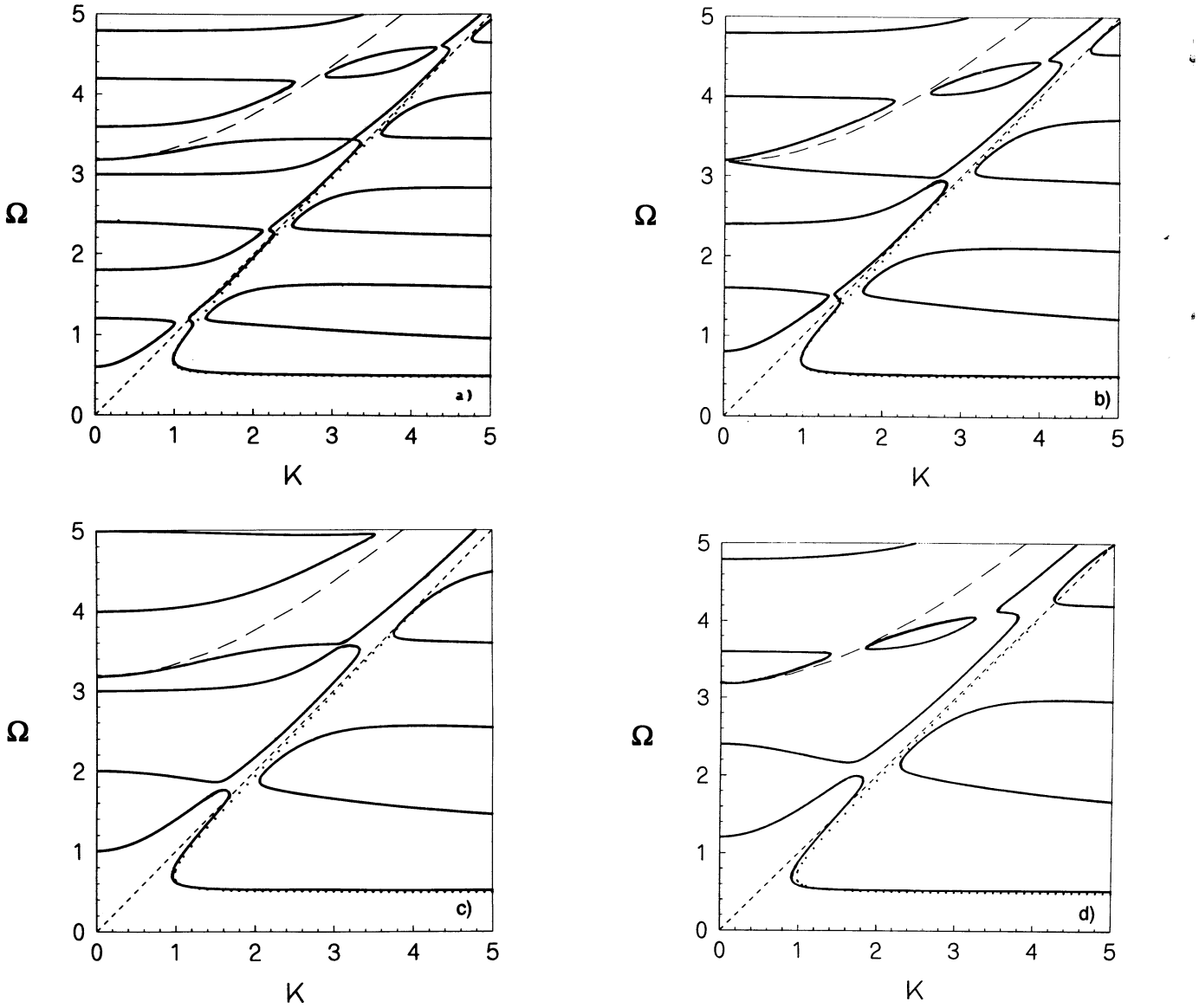

FIG. 8.—Evolution of the K-Ω diagram with increasing ϵ, for $D = 1$, $\gamma = 5/3$, and zero-gradient boundary conditions. The following values of ϵ are shown: (*a*) $\epsilon = 0.15$; (*b*) $\epsilon = 0.20$; (*c*) $\epsilon = 0.25$; (*d*) $\epsilon = 0.30$. The pure Lamb mode ($\Omega = K$) has been shown with a short dashed line, the pure gravity-Lamb mode frequency (given by eq. [15]) is shown by a dotted line, and the pure p_1-mode is shown by a long dashed line.

modes emerge and continue toward higher K. The same pattern of behavior is repeated near the subsequent intersection points, such as the m_3- and m_4-modes also shown in Figure 7*b*; however, here the separation between the Lamb and the gravity-Lamb modes is so small that the two sets of avoided crossings almost merge.

Another interesting feature of this analysis concerns the lowest possible frequency of the normal modes, for a weak field. In Paper I, we found that this is given by the m_1-mode. However, in the present case the lower cutoff is given by the smaller of the m_1 and the gravity-Lamb mode frequencies. This behavior persists even as we increase the strength of the magnetic field, as can be seen in Figures 8*a*–8*d*, where we present the K-Ω diagram for $\epsilon = 0.15$, 0.20, 0.25, and 0.30. The short-dashed and dotted lines depict the pure Lamb and gL-modes, respectively. With increasing ϵ, the frequencies of the magnetic modes increase, but the gL-mode is unmodified with frequency $\Omega \rightarrow \Omega_{BV}$ for large K.

5.3. *Avoided Crossings between p-Modes, Magnetic Modes, and the Gravity-Lamb Mode*

The situation becomes further complicated when interactions involving the p-modes are considered. This is also illustrated in Figures 8*a*–8*d*, where the long-dashed line shows the p_1-mode in the nonmagnetic case. With increasing ϵ the frequencies of the magnetic modes shift past the p-mode frequencies, leading to shifting patterns of avoided crossings. Particularly striking is the formation of "islands" of modes which drift toward higher K; this is visible, for example, in Figures 8*c* and 8*d*. Also, the connectivity of the eigencurves changes. This is illustrated in more detail in Figure 9, corresponding to values of ϵ intermediate between those for Figures 8*a* and 8*b*. It is evident that there are values of ϵ where an actual crossing of the curves take place, leading to degeneracy in

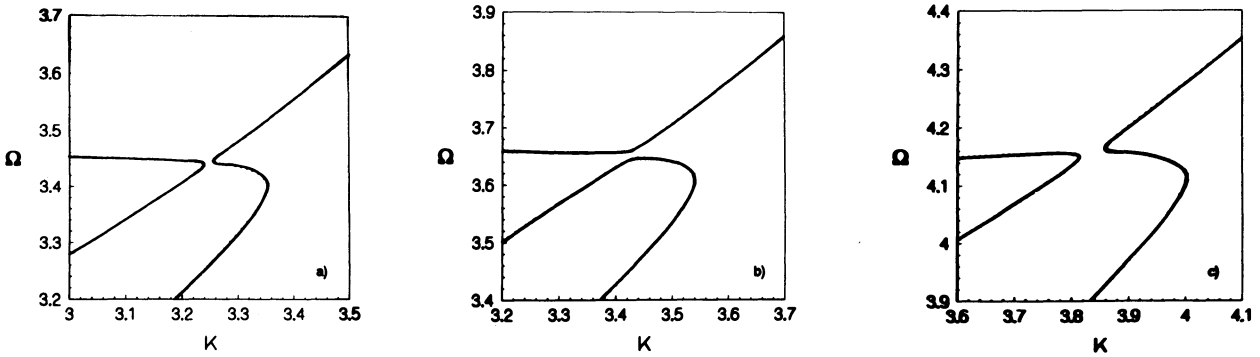

FIG. 9.—Details of the changes in the connectivity of the K-Ω diagram with ϵ, for $D = 1$, $\gamma = 5/3$, and zero-gradient boundary conditions. The following values of ϵ are shown: (*a*) $\epsilon = 0.15$; (*b*) $\epsilon = 0.16$; (*c*) $= 0.185$.

the eigenspectrum. Although we have not analyzed this behavior further, it appears to be linked to the interaction, even though fairly distant, with the p_1-mode.

The development of the K-Ω diagram for somewhat stronger field, corresponding to $\epsilon = 0.5$, is illustrated in Figure 10. Here the dashed curves correspond to the zero-displacement boundary conditions of Paper I, and the continuous lines represent the zero-gradient boundary conditions. In the latter case the lowest two magnetic modes m_1 and m_2, the lowest p-mode p_1, and the gravity-Lamb mode are present. The behavior of the mode coupling is drastically different in the two cases. In the zero-displacement case, the avoided crossing occurs through the interaction of a Lamb-modified magnetic mode with a p-mode, which results in a conversion of a modified m_1-mode to a p_1-mode and vice versa. On the other hand, for the zero-gradient boundary conditions the gravity-Lamb mode merges with the m_1- and the p_1-modes, in a manner similar to Figure 8. In fact, near the avoided crossing the coupling is here between three different modes, namely the p_1-, the modified m_1-, and the gravity-Lamb mode; thus, the coupling cannot be explained in terms of the two-mode coupling analyzed so far. To the right of the intersection points we find, similar to the behavior in Figure 8, the appearance of the m_1 and p_1 branches. At higher K, the behavior is similar to that found for rigid boundary conditions.

Another interesting feature of the results, visible in Figures 8 and 10, is that as ϵ increases the gL-mode starts crossing the $\Omega = K$ line. In this region of the diagram, the mode begins to feel the increasing effects of the magnetic field, and its classification as a gL-mode is not fully appropriate: thus, the validity of equation (15) is questionable. However, on the basis of a local treatment it appears that the appropriate generalization of equation (15) is

$$\Omega^4 - (\epsilon^2 + 1)K^2\Omega^2 + \Omega_{BV}^2 K^2 = 0 . \tag{38}$$

This expression is taken from the analysis by Nagakawa et al. (1973) for trapped magnetoatmospheric waves, based on the use of a WKB approximation. Nagakawa et al. examined the domain of trapped magnetoatmospheric waves and obtained (38) as the equation of one of their boundary curves. Moreover, their K-Ω diagram shows this branch. The main concern of these authors was to find out the domains of trapped waves, but they did not identify the branch corresponding to equation (38) as a gravity-Lamb mode (or, more accurately, a magneto-gravity Lamb mode) for moderate to strong fields. From equation (38) we find that

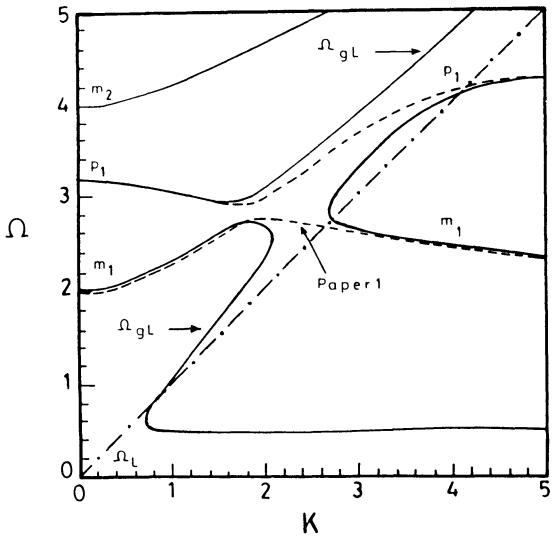

FIG. 10.—Details of avoided crossings in the diagnostic diagram between the p_1-mode, magnetic modes, and Lamb mode for $\epsilon = 0.5$, corresponding to moderate field strength. Solid curves are for the zero-gradient boundary conditions, and dashed curves are for the rigid boundaries used in Paper I.

asymptotically, in the limit of large K, $\Omega \simeq (1 + \epsilon^2)^{1/2}K$ on the upper branch of this mode, and for the lower branch, that $\Omega \simeq \Omega_{BV}/(1 + \epsilon^2)^{1/2}$. The quantitative agreement of this asymptotic behavior with the numerical results is discussed in the next section.

6. K-Ω DIAGRAM FOR STRONG FIELDS

We consider now an isothermal atmosphere extending over several scale heights for which $v_A \gg c_s$ over most of the atmosphere. This situation is somewhat similar to the atmosphere in a sunspot. First we classify the elementary wave modes present in such an atmosphere for zero-gradient boundary conditions and examine their behavior in the diagnostic diagram. Our main emphasis will be on the properties of the gravity Lamb mode in a strong field.

6.1. *Modes in the Strong-Field Case*

Figures 11*a* and 11*b* show the diagnostic diagram corresponding to $D = 5.0$, $\epsilon = 0.8$ and $D = 10.0$, $\epsilon = 0.5$. The solid lines were obtained by solving equation (6) numerically. We consider first the solution for small K. There are two families of solutions, which correspond to slow magnetoacoustic modes or p-like modes with frequencies given by

$$\Omega_{p,n} = \sqrt{\frac{n^2\pi^2}{D^2} + \frac{1}{4}}, \tag{39}$$

and fast magnetoacoustic modes or m-modes with frequencies approximately given by (Scheuer & Thomas 1981)

$$\Omega_{m,l} = \sqrt{\frac{\epsilon^2}{4} j_{2K,l}^2 + K^2}, \tag{40}$$

where $j_{2K,l}$ denotes the lth zero of J_{2K}. Equations (39) and (40) are used to classify the modes close to $K = 0$ in the diagnostic diagram. Note that, unlike the weak-field case, the p-mode frequencies are essentially independent of K: the p-modes are indicated by the nearly horizontal dotted curves in the diagnostic diagram. Equation (40) suggests that m-mode eigencurves, indicated by dashed curves in the diagnostic diagram, are nearly parabolic.

Unlike Paper I, in which the p_1-mode provided a cutoff for the lowest possible frequency of the system for this set of parameters, we also find the presence of the gL-mode below this cutoff for large magnetic field. The avoided crossings around the K-Ω line in Figures 11*a* and 11*b* are a result of the interaction between the gL-mode and p-modes. In Figure 11*a* the gL-mode crosses the Ω-K line because of the strong magnetic field (see the discussion following eq. [38]), and when it comes close to the p_1-mode it merges with it. The dot-dashed curve represents the solution of equation (38); it is interesting to note that the asymptotic limits are in quantitative agreement with the numerical results. Because of the strong magnetic field effect, the pure gL-mode modifies into a magneto gravity-Lamb mode or MgL-mode. The MgL-mode reappears again away from the avoided crossing, and the same behavior is repeated. On the other hand, the m_1-mode and p_3-mode undergo a mode transformation in the usual way.

Magnetoatmospheric waves for the strong magnetic field were studied by Abdelatif (1990). To compare the results of the two analyses, we concentrate on Figure 11*b*, which can be compared with Figure 3 of Abdelatif (1990). One easily identifies the gL-mode near the $\Omega = K$ line; in fact, equation (40) shows that there are no m-modes in that part of the diagnostic diagram. Abdelatif did not

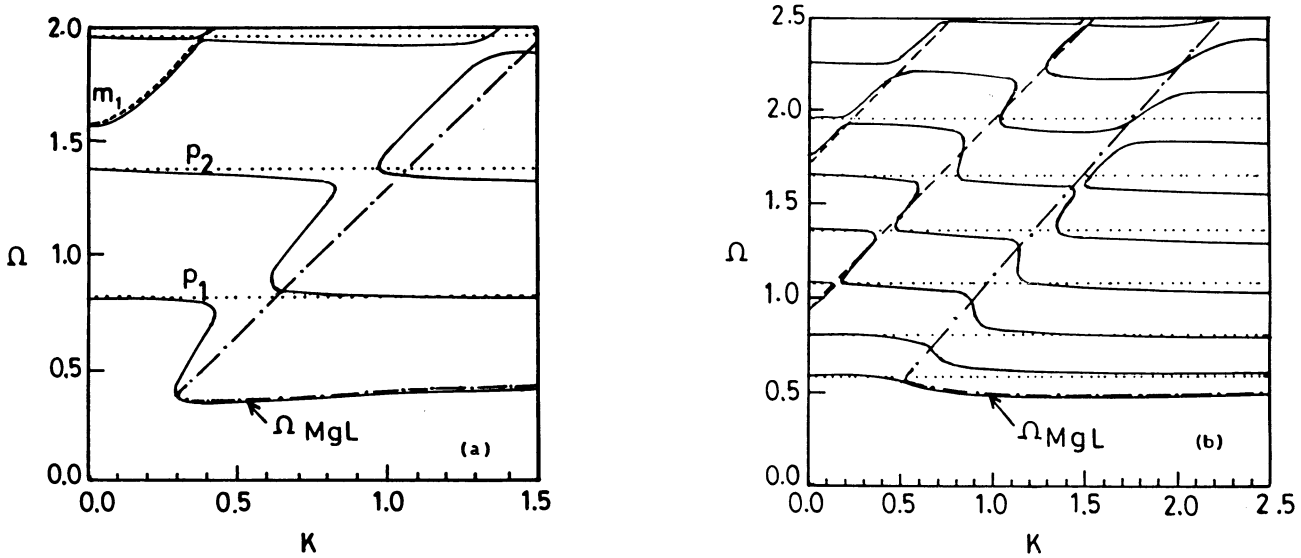

FIG. 11.—Variation of Ω with K in an isothermal atmosphere in the strong magnetic field case. The classification of the modes into p- and m-type refers to the solutions of eq. (39) and (40), respectively, for $K = 0$. Dotted curves represent the p-type solutions, and dashed curves represent the m-type solutions. The magnetogravity Lamb mode (corresponding to the solution of eq. [38]) is represented by the dot-dashed line labeled as Ω_{MgL}. (*a*) $D = 5.0$, $\epsilon = 0.8$; (*b*) $D = 10$, $\epsilon = 0.5$.

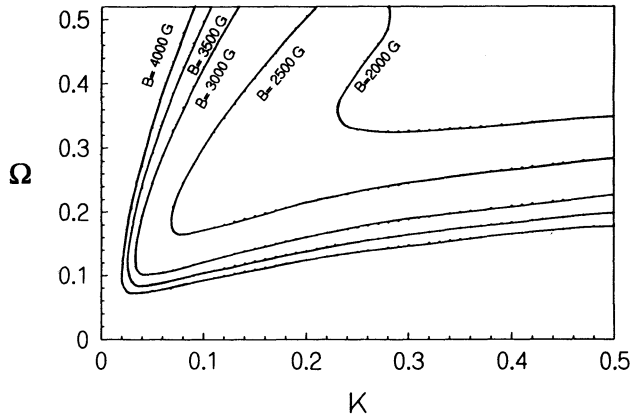

FIG. 12.—Region in the diagnostic diagram for $D = 20$ and different field strengths, as labeled. Only the MgL-mode is present.

recognize the presence of the MgL-mode and, moreover, he did not interpret correctly the interaction of this branch with the p-modes. The avoided crossings in other parts of Figure 11*b* can be explained in terms of interaction between p-modes and m-modes in the usual way.

6.2. *Umbral Oscillations*

It is well known from observations that oscillations in sunspot umbrae typically have periods in the range 2–3 minutes. The lower layers of the umbral atmosphere are found to have maximum power in the 5 minute range, while the chromosphere and transition region have periods in the range 120–200 s.

Our results on the MgL-mode may be applied to oscillations in the atmosphere of a sunspot umbra, which we idealize as an isothermal layer of vertical extension $D = 20$. For $c_s = 6.5$ km s^{-1} (corresponding to a scale height of 100 km), the upper boundary is at a height of 2000 km, which corresponds roughly to the chromosphere in a sunspot. The sharp increase in temperature in these layers provides a natural reflection for the modes. Figure 12 shows the MgL-mode in the K-Ω diagram for various values of ϵ or the field strength B, which are used to label the curves. We do not show the p-modes in the figure, since their spectrum is essentially the same as that shown in Figure 10 of Paper I.

The curves depicted in Figure 12 follow closely the dispersion relation given by equation (38). An interesting point to note here is that with increasing magnetic field strength, the MgL-mode resembles more a magnetic mode than a pure gL-mode. We determine now the eigenfrequencies of the MgL-mode for a typical umbral radius in the range 3000–7000 km and magnetic field between 2000–4000 G. Table 1 presents the eigenfrequencies of the MgL-mode obtained from our model atmosphere with $D = 20$. Following Scheuer & Thomas (1981), let us treat the sunspot umbra as a cylinder of radius a. It can easily be shown that our analysis for a plane can be carried over in a straightforward way to axisymmetric modes in cylindrical geometry and regarding ξ_x and k as the radial displacement and wavenumber, respectively. Assuming that the radial component of the displacement vanishes at $r = a$, we find that k takes discrete values given by $ka = j_{1,\nu}$, where $j_{1,\nu}$ denotes the zero of the Bessel function J_1 of order ν. We consider the

TABLE 1

EIGENFREQUENCIES OF THE MgL-MODE FOR DIFFERENT RADII AND MAGNETIC FIELD STRENGTH OF A SUNSPOT UMBRA

a (km)	B (G)	ω (s^{-1})	P (s)
3000.....	2500	0.0228	275
	3000	0.0317	198
3500.....	2500	0.0212	297
	3000	0.0298	211
	3500	0.0343	183
4000.....	2500	0.0198	317
	3000	0.0278	226
	3500	0.0324	194
5000.....	2500	0.0145	432
	3000	0.0224	280
	3500	0.0267	235
	4000	0.0298	211
6000.....	3000	0.0209	301
	3500	0.0250	251
	4000	0.0293	214
7000.....	3000	0.0172	365
	3500	0.0208	302
	4000	0.0234	268

lowest order mode (where order here is with respect to the horizontal direction) corresponding to $\nu = 1$. This provides us with a relation between the horizontal wavenumber and radius of the spot.

Thus, we see that for field strengths and radii typical for sunspots, the MgL-mode has periods in the observed range. It should also be noted that the lowest order fast magnetoacoustic mode or m_1-mode appears at $\Omega = 0.8$, which corresponds to a period of 119 s. Though our model atmosphere is somewhat idealized, we show that the MgL-mode may be relevant to umbral oscillations.

7. DISCUSSION

The present analysis has revealed many interesting features regarding wave propagation in a stratified media. As in Paper I, we have largely concentrated our analysis on the weak-field limit ($v_A/c_S = \epsilon \ll 1$) and extended the previous calculations to different types of boundary conditions. For $v_A/c_S \ll 1$, the character of the waves can be analyzed in terms of elementary modes of a non-magnetic atmosphere and pure magnetic modes. Our analysis confirms the result found in Paper I that, to lowest order in ϵ, the magnetic Lamb mode is also a solution. As noted in Paper I, the Lamb mode is not a mode of nonmagnetic atmosphere, since it does not satisfy the boundary conditions. However, this becomes possible in the presence of a magnetic field, through a slight coupling with the magnetic modes via the boundary conditions.

Our treatment of the weak-field limit has permitted an analysis of the K-Ω diagram in terms of asymptotic approximations; this has allowed us to understand the nature of the modes in a vertical magnetic field. The insight so gained has proved useful in extending the computations to the moderate- to strong-field case.

A new feature of the present analysis is the occurrence of an additional mode. For larger K, this mode has one branch merging with Ω_{BV} and a second branch which is close to the pure Lamb mode; this leads us to refer to it as a gravity-Lamb mode (see Fig. 7*b*). It is striking that the gravity-Lamb mode is also a solution in a nonmagnetic atmosphere for zero-gradient boundaries. In the asymptotic description, the mode arises from a factor $K_z^2 + \frac{1}{4}$ in the dispersion relation (eq. [B10]) which seems to persist to fairly high asymptotic order. We do not find the presence of this mode for other sets of boundary conditions used in Paper I and in this paper as well. The main emphasis of this work has been on the properties of this mode. We have extended our analysis to moderate to strong fields also and find that the gravity-Lamb mode becomes modified as a magnetogravity-Lamb mode. As a result of the influence of the strong magnetic field, it crosses the pure Lamb mode and merges with the magnetic modes (Figs. 8 and 10). The identification and interaction of this mode with other modes do not appear to have been carried out earlier, despite the fact that it appears in the local analysis of Nagakawa et al. (1973). However, the results of a local analysis, which do not take into account boundary conditions, should be viewed with caution (Thomas 1982). Our results based on a rigorous approach confirm that the gL-mode is present in the special case of vanishing gradient boundary conditions, but not for all sets of boundary conditions.

Another aspect of the results regards the influence of the magnetic field on the dense spectrum of g-like modes. The analysis of Paper I revealed that the entire low-frequency spectrum of g-modes below the frequency of the m_1-mode is effectively eliminated by the magnetic field. As the magnetic field increases, the lower threshold frequency can become larger than the Brunt-Väisälä frequency for rigid boundary conditions. In this case, we find that it is the Brunt-Väisälä frequency which provides the lower cutoff. Thus, even when the magnetic field becomes large, there is always a gravity-like mode present at large K.

The present calculations also demonstrate that when the same reflecting boundary conditions are used at the top and the bottom of the layer, the overall nature of the frequency spectrum, at least for weak fields is insensitive to the precise form of the boundary conditions, away from the avoided crossings; an exception is the gL-mode, which exists only when the gradients vanish at both boundaries. However, the qualitative nature of mode interaction close to the intersection point can be sensitive to the boundary conditions. This feature appears to hold even for strong fields. The use of mixed boundary conditions (zero displacement on one boundary and zero gradients on the other) introduces a frequency shift in the m-, p-, and g-modes corresponding approximately to half the frequency separation between adjacent modes.

The change of the boundary conditions has a striking effect on the connectivity of the eigencurves at avoided crossings, relative to the results obtained in Paper I with zero-displacement conditions. This was already noticeable in the results of Abdelatif (1990). The zero-displacement boundary conditions provide real solutions for the frequency Ω at all wavenumbers K; in contrast, calculations with zero-gradient conditions at both or one of the boundaries lead to complex-conjugate pairs of roots for Ω when K is in the vicinity of some or all of the avoided crossings. In terms of the real solutions, the avoidance happens in K rather than in Ω. This behavior can be understood from asymptotic analysis of the solution near the avoided crossings. A mathematically analogous phenomenon was found by Lee & Saio (1990) in the case of coupling between stellar pulsation and rotation. It is obvious that one of the complex branches of Ω corresponds to overstable modes. In the case of rotating stars, the growth of the mode results from a transfer of energy from rotation to the pulsation, as noted by Lee & Saio. In the present case, the energy input to the growing mode must presumably occur at the boundaries, but the physical details of this process so far elude us. For mixed boundary conditions the behavior is superficially similar, although the minimum separations in the avoided crossings are substantially larger, leading to extensive regions in the diagnostic diagram where no modes are found.

Oscillations in a realistic stellar atmosphere are affected by radiative dissipation and energy loss at the boundaries. Thus the modes are damped, with complex frequencies. The effects on the topology of the K-Ω_r diagram (Ω_r being the real part of the frequency) in the vicinity of an avoided crossing depend on the relative magnitude of the damping rates of the two modes involved and the minimum separation in the (undamped) avoided crossing (Christensen-Dalsgaard 1981). If the minimum separation exceeds the difference in damping rates between the modes, Ω_r undergoes an avoided crossing, while the damping rates cross. On the other hand, if the difference in damping rates exceeds the minimum separation, the avoided crossing of the undamped modes is converted to an actual crossing.

It is appropriate to mention that the main thrust of our investigation has been to examine the physics of wave propagation in a stratified atmosphere with a vertical magnetic field. One of our objectives has been to examine the modal structure and see how it is influenced by the field. These studies of modal physics form a useful background for physically more realistic situations. In Paper I,

we used a specific set of boundary conditions to study this problem. We have now extended the previous results to different boundary conditions and seen how they influence the various modes. We have also demonstrated that the new *MgL*-mode has periods that fall within those observed in umbral oscillations. In forthcoming investigations, we hope to enlarge further the scope of our analysis to more realistic conditions, especially to consider wave leakage from the boundaries. For polytropic and sunspot atmospheres, this problem has been studied by Cally & Bogdan (1993) and Cally, Bogdan, & Zweibel (1994). Following Spruit & Bogdan (1992), slow modes are allowed to drain energy by propagating downward through the bottom boundary. This provides an effective method of absorbing energy from external *p*-modes, by the coupling between these modes in layers where the sound and Alfvén speeds are comparable. However, a careful analysis of the effect of the field on the modal structure still needs to be carried out. This we hope to attempt in subsequent papers. We expect that study of the present kind of mode physics will also help us in understanding heating in active regions through the process of mode conversion.

We are grateful to an anonymous referee for perceptive comments on an earlier version of the text. This work was supported in part by the Danish National Research Foundation through its establishment of the Theoretical Astrophysics Center.

APPENDIX A

SOLUTION OF EQUATION (6)

Here we present the asymptotic properties of the solution of the wave equations in a uniform vertical magnetic field. It was shown by ZD that the general solution to equation (6) can be expressed in terms of Meijer functions as follows:

$$\xi_x^{(h)} = G^{12}_{2,4}\left(\mu_h, \begin{matrix} a_1 & , & a_2 \\ \mu_1, \ \ldots, & \mu_i, \ \ldots, & \mu_4 \end{matrix} \middle| \theta^2\right) \qquad (i, h = 1, \ldots, 4; \quad i \neq h)\,, \tag{A1}$$

where

$$\mu_{1,2} = \frac{(1 \pm i\alpha)}{2}\,, \qquad \mu_{3,4} = \pm K\,, \tag{A2}$$

$$a_{1,2} = \frac{(1 \pm \phi)}{2}\,, \tag{A3}$$

$$\alpha = \sqrt{4\Omega^2 - 1}\,, \tag{A4}$$

$$\phi = \sqrt{-\alpha^2 + 4K^2(1 - \Omega_{\rm BV}^2/\Omega^2)}\,, \tag{A5}$$

and $\Omega_{\rm BV}^2 = (\gamma - 1)/\gamma^2$ is the Brunt-Väisälä frequency (in dimensionless units).

Once $\xi_x^{(h)}$ is known, it is fairly straightforward to determine the corresponding solutions $\xi_z^{(h)}$ from either of equations (1) or (2). The complete solutions satisfying the required boundary conditions can be built up as linear combinations of $\xi_x^{(h)}$ and $\xi_z^{(h)}$.

APPENDIX B

WEAK-FIELD SOLUTIONS

We now focus our attention on the limit of a weak field, for which $c_S/v_A \gg 1$ and $\theta \gg 1$. This corresponds to the limit of small ϵ, with

$$\epsilon \equiv \frac{v_{A,0}}{c_S}\,. \tag{B1}$$

In addition, however, we must require that the vertical extension d of the layer is not too large (see eq. [5] (for $d > 0$). Since the density increases for negative z, the above restriction, of course, does not apply if d lies below the plane $z = 0$.

When $\theta \gg 1$, the Meijer function in equation (A1) has the following asymptotic expansion (ZD):

$$G^{12}_{2,4}(\mu_h \mid \theta^2) = \frac{1}{2\sqrt{\pi\theta}}\left[e^{i(2\theta - \delta_h)}\left(1 + i\,\frac{M}{\theta} - \frac{M_1}{\theta^2}\right) + e^{-i(2\theta - \delta_h)}\left(1 - i\,\frac{M}{\theta} - \frac{M_1}{\theta^2}\right)\right]$$
$$+ \frac{1}{\theta}\left[S_h\left(1 + \frac{L_1^+}{\theta^2}\right)\theta^{2iK_z} + T_h\left(1 + \frac{L_1^-}{\theta^2}\right)\theta^{-2iK_z}\right] + O\left(\frac{1}{\theta^3}\right), \tag{B2}$$

where K_z^2, δ_h, M, M_1, $L_1^{\pm}$, $w_{\pm}$, S_h, and T_h are all defined in Paper I.

Using the expansion given by equation (B2), we find that $\xi_x^{(h)}$ and $\xi_z^{(h)}$ can be expressed in a compact form as follows:

$$\xi_x^{(h)} = \frac{1}{\theta}\sum_{j=1}^{2} C_j^{(h)} f_j(\theta) + \frac{1}{\sqrt{\theta}}\sum_{j=3}^{4} C_j^{(h)} f_j(\theta)\,, \tag{B3}$$

$$i\xi_z^{(h)} = \frac{1}{\theta}\sum_{j=1}^{2} C_j^{(h)} g_j(\theta) + \frac{1}{\theta^{3/2}}\sum_{j=3}^{4} C_j^{(h)} g_j(\theta)\,, \tag{B4}$$

where $C_j^{(h)}, f_j^{(h)}$, and $g_j^{(h)}$ are defined in Paper I. It follows that the gradients can be expressed as

$$\frac{d\xi_x^{(h)}}{dz} = \frac{1}{\theta}\sum_{j=1}^{2} C_j^{(h)}\left[\frac{f_j(\theta)}{2H} + \frac{df_j(\theta)}{dz}\right] + \frac{1}{\sqrt{\theta}}\sum_{j=3}^{4} C_j^{(h)}\left[\frac{f_j(\theta)}{4H} + \frac{df_j(\theta)}{dz}\right], \tag{B5}$$

$$i\frac{d\xi_z^{(h)}}{dz} = \frac{1}{\theta}\sum_{j=1}^{2} C_j^{(h)}\left[\frac{g_j(\theta)}{2H} + \frac{dg_j(\theta)}{dz}\right] + \frac{1}{\theta^{3/2}}\sum_{j=3}^{4} C_j^{(h)}\left[\frac{3g_j(\theta)}{4H} + \frac{dg_j(\theta)}{dz}\right]. \tag{B6}$$

To derive the dispersion relation, we now apply the boundary conditions given by equation (7) to equation (B5) and (B6). We obtain a set of four equations which can be written as

$$AX = 0\,, \tag{B7}$$

where

$$X^T = (C_1 \quad C_2 \quad C_3 \quad C_4)\,,$$

and

$$A = \begin{bmatrix}
\left(\frac{f_1}{2H} + \frac{df_1}{dz}\Big|_0\right)\Big/\theta_0 & \left(\frac{f_2}{2H} + \frac{df_2}{dz}\Big|_0\right)\Big/\theta_0 & \left(\frac{f_3}{4H} + \frac{df_3}{dz}\Big|_0\right)\Big/\theta_0 & \left(\frac{f_4}{4H} + \frac{df_4}{dz}\Big|_0\right)\Big/\theta_0 \\
\left(\frac{f_1}{2H} + \frac{df_1}{dz}\Big|_D\right)\Big/\theta_D & \left(\frac{f_2}{2H} + \frac{df_2}{dz}\Big|_D\right)\Big/\theta_D & \left(\frac{f_3}{4H} + \frac{df_3}{dz}\Big|_D\right)\Big/\theta_D & \left(\frac{f_4}{4H} + \frac{df_4}{dz}\Big|_D\right)\Big/\theta_D \\
\left(\frac{g_1}{2H} + \frac{dg_1}{dz}\Big|_0\right)\Big/\theta_0 & \left(\frac{g_2}{2H} + \frac{dg_2}{dz}\Big|_0\right)\Big/\theta_0 & \left(\frac{3g_3}{4H} + \frac{dg_3}{dz}\Big|_0\right)\Big/\theta_0 & \left(\frac{3g_4}{4H} + \frac{dg_4}{dz}\Big|_0\right)\Big/\theta_0 \\
\left(\frac{g_1}{2H} + \frac{dg_1}{dz}\Big|_D\right)\Big/\theta_D & \left(\frac{g_2}{2H} + \frac{dg_2}{dz}\Big|_D\right)\Big/\theta_D & \left(\frac{3g_3}{4H} + \frac{dg_3}{dz}\Big|_D\right)\Big/\theta_D & \left(\frac{3g_4}{4H} + \frac{dg_4}{dz}\Big|_D\right)\Big/\theta_D
\end{bmatrix}. \tag{B8}$$

Here $\theta_0 = \theta(0)$ and $\theta_D = \theta(D)$. The condition for equation (B8) to have a nontrivial solution is

$$\det\,[A] = 0\,. \tag{B9}$$

Expanding equation (B9) and substituting for f_j and g_j ($j = 1, \ldots, 4$) from Paper I we obtain

$$\begin{aligned}
\left(\frac{1}{4} + K_z^2\right)(\Omega^2 - K^2)\sin\tilde{\theta}\sin(K_z D) = {} & 2\frac{\epsilon}{\Omega}e^{D/4}\left(\frac{1}{4} + K_z^2\right)\left\{K_z K^3\left[\cosh\left(\frac{D}{4}\right)\cos\tilde{\theta}\cos(K_z D) - \cosh\left(\frac{D}{2}\right)\right]\right. \\
& \left. + \sinh\left(\frac{D}{4}\right)\cos\tilde{\theta}\sin(K_z D)\left[\left(M + \frac{1}{4}\right)(\Omega^2 - K^2) - K^3\left(\frac{1}{\gamma} - \frac{1}{2}\right)\right]\right\} \\
& + \frac{\epsilon^2}{\Omega^2}e^{D/2}\sin\tilde{\theta}\left(\frac{1}{4} + K_z^2\right)\left[\left[M(M+2)(K^2 - \Omega^2) + 2MK^3\left(\frac{1}{\gamma} - \frac{1}{2}\right) - rK^4\right]\sin(K_z D)\right. \\
& + 2K^2\left[u_- + \left(NK + \frac{3}{4}\right)K_z\right]\sinh\left(\frac{D}{2}\right)\cosh(K_z D) \\
& \left. + 2\left\{\left(M_1 + \frac{3}{4}\right)(\Omega^2 - K^2) + K^2\left[\frac{u_+}{i} + \left(\frac{1}{\gamma} - \frac{1}{2}\right)\left(\frac{3}{4} + KN\right)\right]\right\}\cosh\left(\frac{D}{2}\right)\sin(K_z D)\right] \\
& + O\left(\frac{\epsilon^3}{\Omega^3}\right),
\end{aligned} \tag{B10}$$

which is the disperson relation accurate to second order in ϵ. Here $\tilde{\theta} = \theta_D - \theta_0$, and M, M_1, N, r, K_z, and $u_\pm$ are given in Appendix B of Paper I.

REFERENCES

Abdelatif, T. E. 1990, Solar Phys., 129, 201
Beckers, J. M., & Schulz, R. B. 1972, Solar Phys., 27, 61
Cally, P. S., & Bogdan, T. J. 1993, ApJ, 402, 721
Cally, P. S., Bogdan, T. J., & Zweibel, E. G. 1994, ApJ, 437, 505
Cash, J. R., Moore, D. R. 1980, Bol. Inst. Tonantzintla, 44
Christensen-Dalsgaard, J. 1981, MNRAS, 194, 229
Ferraro, V. C., & Plumpton, C. 1958, ApJ, 127, 459
Giovanelli, R. G., Harvey, J. W., & Livingston, W. C. 1978, Solar Phys., 59, 40
Hasan, S. S., & Abdelatif, T. 1990, in Physics of Magnetic Flux Ropes, ed. C. T. Russell, E. R. Priest, & L. C. Lee (AGU Monograph No. 58), 93
Hasan, S. S., & Christensen-Dalsgaard, J. 1992, ApJ, 396, 311 (Paper I)
Lee, U., & Saio, H. 1990, ApJ, 360, 590
McLellan, A., & Winterberg, F. 1968, Solar Phys., 4, 401
Moore, R. L., & Rabin, D. 1985, ARA&A, 23, 239
Nagakawa, Y., Priest, E. R., & Wellck, R. E. 1973, ApJ, 184, 931
Scheuer, M. D., & Thomas, J. H. 1981, Solar Phys., 71, 21
Spruit, H. C., & Bogdan, T. J. 1992, ApJ, 391, L109
Thomas, J. H. 1982, ApJ, 262, 760
Uchida, Y., & Sakurai, T. 1975, PASJ, 27, 259
Wood, W. P. 1990, Sol. Phys., 128, 353
Zhugzhda, Yu. D. 1979, Soviet Astron., 23, 42
Zhugzhda, Yu. D., & Dzhalilov, N. S. 1982, A&A, 112, 16 (ZD)
———. 1984a, A&A, 132, 45
———. 1984b, A&A, 132, 52